RESEARCH PAPER

The preparation and characterization of silicon-based composites doped with $BaSO_4$, WO_3, and PbO nanoparticles for shielding applications in positron emission tomography (PET) and nuclear medicine facilities

Reza Malekzadeh [1], Vahid Sadeghi Zali [2], Okhtay Jahanbakhsh [2], Murat Okutan[3], Asghar Mesbahi [4]*

[1] *Medical Radiation Sciences Research Team, Tabriz University of Medical Sciences, Tabriz, Iran*
[2] *Department of Nuclear Physics, Faculty of Physics, University of Tabriz, Tabriz, Iran*
[3] *Department of Medical Physics, Oncology Institute, Istanbul University, Istanbul, Turkey*
[4] *Molecular Medicine Research Center, Tabriz University of Medical Sciences, Tabriz, Iran*

ABSTRACT

Objective(s): The present study aimed to design new nanoparticle-based shielding materials for photons used in single-photon emission computed tomography and positron emission tomography facilities.

Materials and Methods: Initially, the mass attenuation coefficients and half value layer (HVL) of the composites were comprehensively investigated based on a silicon rubber containing various ratios of micro- and nano-barium sulfate ($BaSO_4$), lead oxide (PbO), and tungsten oxide (WO_3) particles at 60, 80, 100, 150, 200, 300, 400, 500, and 600 keV photon energies using the MCNP-X6 Monte Carlo (MC) code and WinXCOM software. In the second stage, the composites composed of 10 wt% and 20 wt% WO_3 and PbO particles were constructed in a liquid silicone rubber-based matrix. The mass attenuation coefficients and HVL of the designed shields were experimentally assessed using Cs-137 and Am-241 radioactive sources.

Results: The particles sizes of PbO and WO_3 were within the range of 50-200 nanometers. The MC and measurement results indicated that the linear attenuation coefficients of the composites were augmented with the addition of all the studied nano- and micro-particles. However, the PbO composites had more significant shielding properties compared to the $BaSO_4$ and WO_3 composites.

Conclusion: According to the results, the nanocomposites had better ability to shield γ-rays at both energies compared to the micro-composites.

Keywords: *Nanocomposite, Nanoparticles, Nuclear Medicine, Radiation Shielding*

How to cite this article

Sadeghi Zali V, Jahanbakhsh O, Okutan M, Mesbahi A. The preparation and characterization of silicon-based composites doped with $BaSO_4$, WO_3, and PbO nanoparticles for shielding applications in positron emission tomography (PET) and nuclear medicine facilities. Nanomed J. 2020; 7(4): 324-334. DOI: 10.22038/nmj.2020.07.00009

INTRODUCTION

Nuclear medicine (NM) has been a fundamental imaging modality that uses radioactive tracers (radiopharmaceuticals) for the assessment of physical functions, as well as the diagnosis and treatment of diseases in several medical specialties [1]. Considering its widespread use, the number of NM procedures increased from 23.5 to 32.7 million worldwide during 1984-2007 and from seven to 18.6 million only in the United States [2]. Single-photon emission computed tomography (SPECT) and positron emission tomography (PET) are common NM imaging procedures that employ gamma-emitting radioisotopes. Nowadays, the use of PET in combination with computed tomography (CT) has become the primary modality for the diagnosis of oncologic diseases. Due to radiation hazards, PET requires special consideration due to the γ-rays (511 keV) that are generated by positron-emitter fluorine-18 [3]. Therefore, it seems that radiation protection plays a critical role in establishing PET/CT [4], as well as other NM facilities [5]. In terms of radiation protection during NM procedures, various studies have evaluated staff doses in different PET/CT centers [6]. The proper radiation shielding of hot lab and imaging room walls, floors, and ceilings in NM is essential to ensuring the protection and safety of the patients and technicians [7].

* *Corresponding Author Email: amesbahi2010@gmail.com*
Note. This manuscript was submitted on February 10, 2020; approved on April 15, 2020

Table 1. List of Frequently Used Diagnostic and Therapeutic Nuclear Medicine Radionuclides

Diagnostic Radionuclides			Therapeutic Radionuclides		
Isotope $(^{A}_{Z}Elemnt)$	γ-ray Energy (keV)	Half Life	Isotope $(^{A}_{Z}Elemnt)$	γ-ray Energy (keV)	Half Life
^{99}Tc	141	6 h	^{153}Sm	103	46.3 h
^{67}Ga	93	78.7 h	^{103}Pd	357	17 d
^{75}Se	265	120 d	^{131}I	364	8 d
^{103}Ru	497	39.4 d	^{137}Cs	662	30.2 y
^{81m}Kr	191	13 s	^{131}I	610	8.04 d
^{57}Co	122	272 d	^{182}Ta	68	115 d
^{127}Xe	203	36.4 d	^{169}Er	110	9.4 d
^{111}In	245	2.8 d	^{111}In	245	2.83 d
^{123}I	159	13.2 h	^{125}I	35	59.4 d
^{153}Sm	103	47 h	^{117m}Sn	160	13.6 d
^{201}Tl	167	73.1 h	^{198}Au	412	2.7 d

y: years, h: hours, d: days, and s: seconds

Furthermore, proper shielding could significantly attenuate high-energy rays to protect the staff and patients who are at prolonged exposure to the ionization radiation source.

Recently, various types of flexible and environmentally friendly nontoxic lead-free composite shields [8] with metal fillers have been proposed for radiation shielding applications [9-12]. According to the literature, the use of nano-sized particles as fillers in different composites could significantly improve the photon attenuation ability of the composite [13,14]. Moreover, Mahmoud et al. investigated γ-ray shielding properties in the polyethylene-based composites of lead oxide nano-powders, reporting that nanoparticles (NPs) had higher mass attenuation coefficients of up to 15% compared to those made of micro-particles [15]. Table 1 shows some of the widely used radioisotopes in NM-emitting γ-rays. Accordingly, they emit photons with energies within the range of 80-600 keV.

To the best of our knowledge, no studies has proposed a nano-composite material considering this photon energy range to protect staff and patients in nuclear medicine departments. The present study aimed to evaluate the photon attenuation of silicon rubber-based micro- and nano-composites doped with barium sulfate ($BaSO_4$), tungsten oxide (WO_3), and lead oxide (PbO) as fillers with high atomic number and high density.

The calculations were performed using the MCNP-X6 Monte Carlo code and WinXcom software. In addition, micro- and nano-composites based on WO_3 and PbO were selectively fabricated and experimentally assessed using Cs-137 and Am-241 radioactive sources. The effects of particle type, size, concentration, and radiation energy were also analyzed and discussed.

Materials and Methods

Monte carlo simulation code

The Monte Carlo N-particle code (MCNP-X version 2.6.0, Los Alamos National Laboratory cross-section libraries data) was used to determine the γ-ray mass attenuation coefficients of the composite shields [16]. The MCNPX code is a well-known MC code used for the modeling of radiation transmission, interaction of particles with matter, and tracing of all particles in different energies [17].

The entire set of the simulation geometry was inserted into one cylindrical space with the height of 150 centimeters and diameter of 40

centimeters. The transfer of the particles outside the box was of no significance. A surface source with the diameter of five millimeters was defined in the MCNP data card with ERG, PAR, POS, and DIR commands for energy, particle type, position, and direction, respectively [18]. The F4 tally, which scores a flux (n/cm3) of photons entering the detector volume, was used to determine the photon fluence entering the detector cell. Simulations were performed for 20 minutes on a personal computer, and the statistical error of the MC results was considered to be less than 1% for all the calculations.

The accuracy and credibility of the MC model were assessed by comparing the MC results with the data provided by WinXcom for a conventional lead material [19]. Therefore, the linear attenuation coefficients of lead (Pb) were calculated and compared with the standard WinXcom data [20]. Moreover, the mass attenuation coefficient (μ_m) and half value layer (HVL) were determined for all the samples. Finally, the validated input code was used to calculate the radiation mass attenuation coefficients of the nano- and micro-composite shields. Fig 1 shows the simulation geometry setup in detail.

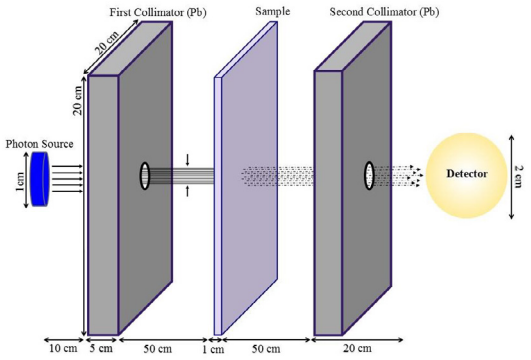

Fig 1. Simulation Geometry of Devolved MCNPX MC Code

In the second stage, $BaSO_4$ ($\rho = 4.5 \frac{g}{cm^3}$), WO_3 ($\rho = 7.16 \frac{g}{cm^3}$), and PbO ($\rho = 9.53 \frac{g}{cm^3}$) in two sizes of spherical particles with diameters of 100 nanometers and 100 micrometers were introduced into silicon rubber in the MCNPX input file. As a result, each nano- and micro-particle was defined using the lattice (LAT) and universe (U) cards of MCNPX [26]. For each composite, the required number of the NPs or micro-particles of $BaSO_4$, WO_3, and PbO to provide the prerequisite weight percentage were calculated. After obtaining the required number of the particles in each composite, the dimensions of a cubic cell surrounding a single filler particle were determined. After scoring the transmitted photons from a specific type of composite with variable thickness, the liner attenuation coefficients were determined based on the Lambert-Beer law, as follows:

$$I = I_0 e^{-\mu x} \qquad (1)$$

In the equation above, I_0 is the intensity of the incident photon beam, I shows the intensity of the transference photon beam, x represents the thickness of the composite, and μ is the linear attention coefficient.

The mass attention coefficient was calculated using the following equation:

$$\mu_m = \frac{\mu}{\rho} \qquad (2)$$

To obtain more data on the shielding properties of the composites, the HVL of the samples was estimated using the following equation:

$$HVL = \frac{Ln\ 2}{\mu} \qquad (3)$$

where μ is the linear attenuation coefficient.

The transmission of mono-energetic γ-rays through the composites at the photon energies of 60, 80, 100, 150, 200, 300, 400, 500, and 600 keV was calculated using narrow beam transmission geometry. The silicon rubber matrix was doped with 10%, 20%, and 40% (wt%) of three fillers. The MC calculations per each energy level were performed in three thicknesses, and a plot of the intensity of the transmitted γ-rays versus thickness was obtained. Following that, the attenuation coefficients were calculated. Table 2 shows the composites as specified by elemental mass fractions and material density.

Experimental procedure

Based on the MC simulation and WinXCom results, WO_3 and PbO were selected for the fabrication of the shielding composites. The selection criteria were based on higher mass attenuation coefficients for the energy range of 80-600 keV.

Preparation of tungsten oxide (WO_3) nanoparticles

In order to synthesize the WO_3 particles, sodium tungstate dehydrate ($Na_2WO_4.2H_2O$) and hydrochloric acid (HCl) were used. Since $Na_2WO_4.2H_2O$ in an acidic medium is faster than other sedimentary environments, HCl was

Table 2. Weight Percentage of Constituent Elements and Density of Simulated and Homemade Composite Shields

Samples	Density ($\frac{g}{cm^3}$)	Weight Percentage (%)							
		Si	O	H	C	S	Pb	W	Ba
100% Si rubber	1.20	10	10	60	20	-	-	-	-
10% $BaSO_4$	1.29	9	15.6	54	18	1.66	-	-	1.66
20% $BaSO_4$	1.40	8	21.3	48	16	3.33	-	-	3.33
40% $BaSO_4$	1.70	6	32.66	36	12	6.66	-	-	6.66
10% PbO	1.31	9	14	54	18	-	5	-	-
20% PbO	1.45	8	18	48	16	-	10	-	-
40% PbO	1.84	6	26	36	12	-	20	-	-
10% WO_3	1.30	9	16.5	54	18	-	-	2.5	-
20% WO_3	1.43	8	23	48	16	-	-	5	-
40% WO_3	1.80	6	36	36	12	-	-	10	-

selected as the precipitate, and distilled water was considered as the solvent. Initially, 10 grams of $Na_2WO_4.2H_2O$ was added to 50 cc of distilled water and stirred homogeneously for two hours using a magnet. Afterwards, 5 cc of HCl (50%) was slowly added to the first solution for two hours. The ratio of $Na_2WO_4.2H_2O$ to distilled water was 1:3, and the ratio of the required HCl for reaction with sodium tungstate dehydrate was 5 cc per 10 grams. The resultant solution was heated at the temperature of 90°C for three hours until becoming yellow. The sediment was dried at the temperature of 400°C for three hours and 450°C for two hours to obtain the WO_3 NPs.

Preparation of lead oxide (PbO) nanoparticles

The PbO NPs were synthesized as follows. For this purpose, 60 ml of aqueous solution of Pb(C2H3O2)2.3H2O (1 M) was prepared using deionized water and heated to the temperature of 90oC. Following that, the solution was added to an aqueous solution containing 50 ml of NaOH (19 M) in a beaker and stirred vigorously. Upon the addition of Pb(C2H3O2)2.3H2O, the solution initially became cloudy and turned deep red afterwards. After stirring for two hours, the red precipitate was filtered and washed with water three times, dried at 100°C for two hours, and calcined at the temperature of 240°C for three hours to obtain the PbO NPs.

Characterization of the nanoparticles

Scanning electron microscopy (SEM; JEOL 6010 and CamScan Apollo 300, Applied Beams, Oregon, USA) was employed to evaluate the shape of the produced particles. In addition, the energy dispersive spectroscopy (EDS) mode of JEOL 6010 was used to assess the element compositions and distribution of the particles in the silicon polymer composites.

Fabrication of the composite shields

After the synthesis of the fillers, the composites with 10% and 20% proportion of PbO and WO_3 weight were prepared using the compression molding technique. Table 2 shows the densities and chemical compositions of the homemade samples. Liquid silicon rubber (LSR) with the chemical components of $Si(CH_3)O$ was selected as the matrix of the composites considering its beneficial properties for the production of radiation shields, particularly thermal and mechanical properties. In this method, the filler and LSR with appropriate proportion were sensitively weighed and mixed thoroughly for the fine dispersion of the filler in a mechanical stirrer for one hour at 50 rpm. After blending, the dispersions were collected from the mixer and poured into circular-shaped plastic molds with the radius of two centimeters and three thicknesses of 0.50, 1.0, and 1.5 centimeters. Following that, they were dried at room temperature (25°C) for

one week [21]. Moreover, SEM-EDS imaging was used to ensure the uniform distribution of the particles within the composite shields.

Measurements of gamma ray transmission

The linear attenuation coefficient μ (cm^{-1}), mass attenuation coefficient μ_m (cm^2/g), and HVL of the PbO and WO_3 composites were determined by measuring the transmission of the γ-rays through the investigated samples with the mentioned thicknesses. The energy of the incident γ-rays used in the current research varied using the two standard radioactive point sources of ^{137}Cs (661.66 keV) and ^{241}Am (59.5 keV). The activity of the mentioned sources was 285 and 210 μCi, respectively on 1 June, 2001. The experiments were performed using a calibrated NaI(Tl) crystal detector (model: GC1520, Canberra). Afterwards, the samples were arranged in front of a collimated beam. The γ-ray source was positioned at the distance of five centimeters from the detector, and the sample was placed at the distance of one centimeter from the γ-ray source.

Statistical analysis

Data analysis was performed in SPSS version 22.0 (IBM Co, Armonk, NY, USA) to determine the values as expressed in mean and standard deviation. All the graphs were developed using GraphPad Prism 6 (GraphPad Co., CA, USA).

RESULTS

In the current research, the μ_m of the silicon rubber-based composites with various loadings of the nano- and micro-sized BaSO4, WO_3, and PbO particles were calculated using the MCNP-X simulation at various photon energies (60, 80, 100, 150, 200, 300, 400, 500, and 600 keV). Additionally, the μ_m of the homemade composite shields with the nano-sized WO_3 and PbO particles was measured using the two radioactive sources of 137Cs and 241Am. Moreover, the HVL of the samples was obtained and compared.

Effects of the photon energy and filler concentration on the mass attenuation coefficients

Figs 2-4 show the calculated mass attenuation coefficients of the samples with various ratios of the filler particles. As can be seen, the values of WinXcom were higher than the values calculated by the MC at all the concentrations.

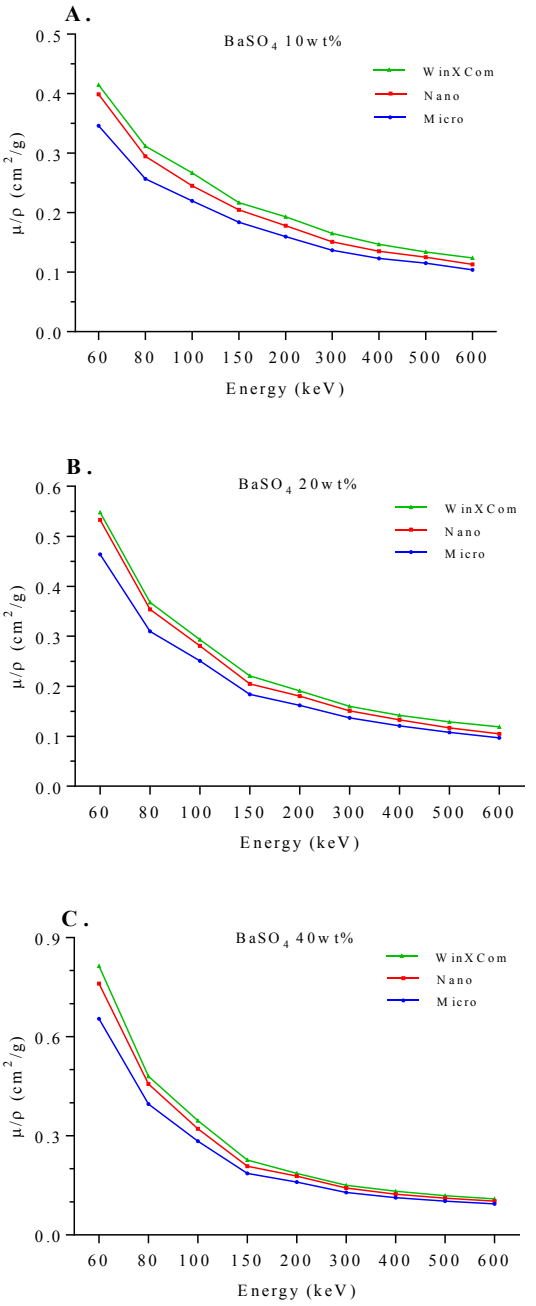

Fig 2. Mass Attenuation Coefficients of Nano- and Micro-$BaSO_4$ Composites at Various Concentrations of BaSO4 as Function of Photon Energy

One of the major reasons could be the approaches utilized by the two programs to calculate the mass attenuation coefficients. In other words, the particle size could not be considered in the WinXcom program, and the atomic state of all the components was considered in the calculations.

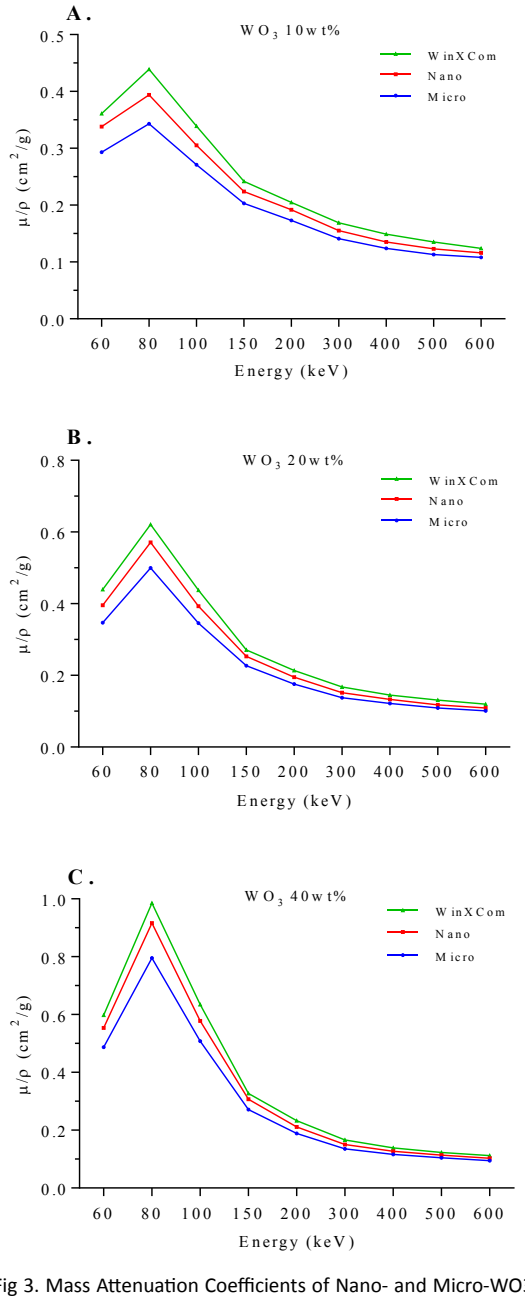

Fig 3. Mass Attenuation Coefficients of Nano- and Micro-WO3 Composites at Various Concentrations of WO_3 as Function of Photon Energy

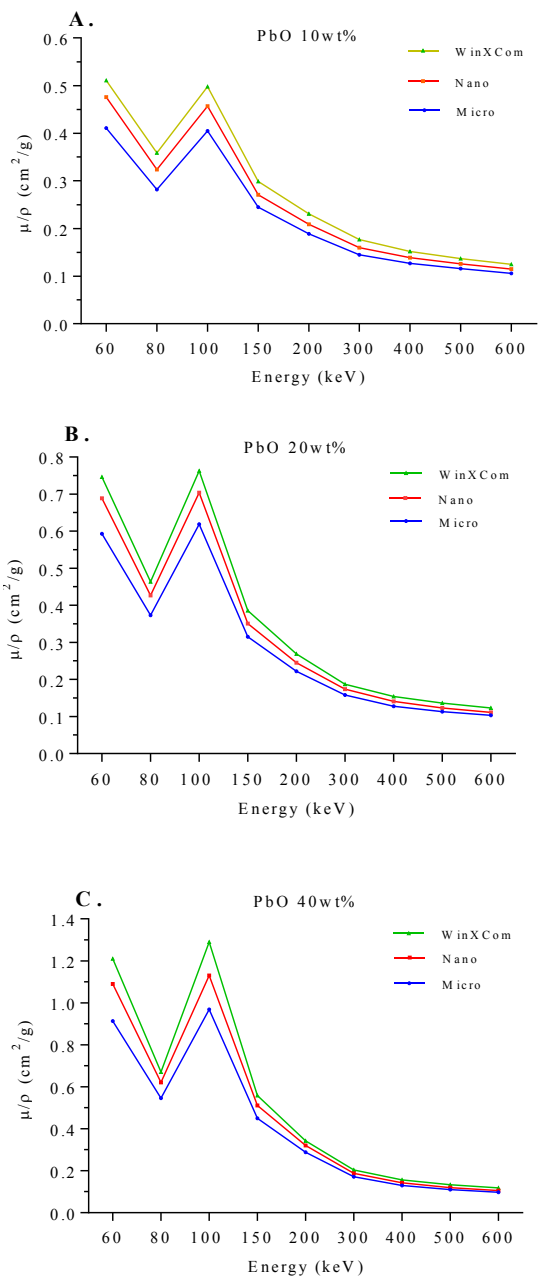

Fig 4. Mass Attenuation Coefficients of Nano- and Micro-PbO Composites at Various Concentrations of PbO as Function of Photon Energy

However, the MC method was applied to determine the physical dimension of the particles by the MC codes. As a result, the small differences in the mass attenuation coefficients between the nano-composites that were calculated by the WinXcom and MC were acceptable.

The mass attenuation coefficients of the studied composites varied based on the chemical compositions of their elements.

As was expected, the maximum values were observed at lower photon energies due to the photoelectric interactions between the photons and filler atoms with high atomic numbers. Afterwards, the values of all the samples decreased rapidly with the increment in the photon energy (up to 600 keV) since the penetration probability of the photons increased with the photon energy (Fig 5).

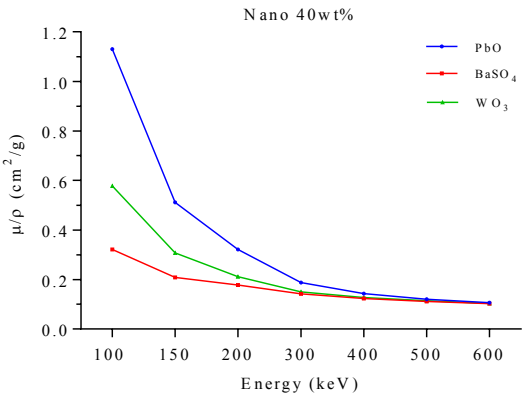

Fig 5. Comparison of mass attenuation coefficients for composites with PbO, BaSO4, and WO3 nanoparticles at same 40 wt% concentration as a function of photon energy

On the other hand, the Compton scattering effect was dominant as the photon energy increased, and the attenuation of the filler atoms depended on the electron density rather than the atomic number. Therefore, the mass attenuation coefficients decreased with the increased γ-ray energies at all the concentrations of $BaSO_4$, WO_3, and PbO, while it improved with the increased filler weight ratio. The MC results also indicated that the nano-sized $BaSO_4$ content decreased from 40% to 10%, while the values decreased from 0.321 to 0.252 cm^2/g at the energy level of 100 keV. Similar findings were also observed in the values, which decreased from 0.578 to 0.305 cm^2/g and from 1.13 to 0.457 cm^2/g at the energy level of 100 keV as the nano-sized WO_3 and PbO contents declined from 40% to 10%.

At the constant filler concentration of 40%, the mass attenuation coefficient of the PbO composite was approximately 3.52 and 1.95 times higher compared to $BaSO_4$ and WO_3 at the energy level of 100 keV and 1.16 and 1.12 times higher compared to the $BaSO_4$ and WO_3 composites at the energy level of 400 keV, respectively. Therefore, the obtained results indicated that the mass attenuation coefficients of the PbO composites were higher compared to the $BaSO_4$ and WO_3 composite shields. Among all the studied composites and concentrations, the composite composed of 40% PbO showed the highest values.

Effect of the particles size on the mass attenuation coefficient

As is shown in Figs 2-4, the mass attenuation coefficients of the micro- and nano-sized $BaSO_4$, WO_3, and PbO composite samples were compared with similar weight percentages of the fillers. In addition, it was observed that the mass attenuation coefficient of the composites decreased with the increased size of the $BaSO_4$, WO_3, and PbO particles. The effect of the particle size could be explained based on the probability of the photon interaction with the particles, which largely depended on the surface-to-volume ratio of the particles that was significantly higher in the NPs compared to the micro-particles. In contrast to the MC code, the WinXcom software considered a composite as the atomic mixtures of its components with the homogenous distribution of the constituent atoms. Therefore, the particle size was not considered in the WinXcom software, and the particle size was evaluated based on the MC results. With respect to the photon energy, $()_{nano}$ was observed to be highest at lower energies, while the increased photon energy from 100 to 600 keV caused the value of $()_{nano}$ to slowly reduce. Consequently, the nano-composites exhibited more effective shielding ability compared to the micro-composites at the same concentration of the $BaSO_4$, WO_3, and PbO particles where the photoelectric process would be the main interaction type between photons and atoms.

The comparison of our findings with similar studies showed a similar investigation conducted by Malekzadeh et al., the results of which indicated that nano-sized Bi composites improved 37-79% of the shielding properties of γ photons at the diagnostic energy range compared to micro-sized Bi composites [18]. This is consistent with the current research in terms of the effects of photon energy and particle size. Moreover, our findings demonstrated that the effect of particle size increased with the filler concentration and decreased with the photon energy.

In another study, Tekin et al. reported that compared to micro-particles, the addition of nano-WO_3 to hematite-serpentine concrete could increase the mass attenuation coefficients by up to 7% and 5.6% for the gamma photons with the energy of 142 and 662 keV [22]. In other words, photons with higher energy slightly decrease the effect of particle size. In an MC experiment performed by Mesbahi et al., the addition of the nano- and micro-particles of PbO_2, Fe_2O_3, WO_3, and H_4B to ordinary concrete was reported to increase absorbed radiation in the attenuator material. Furthermore, the mentioned research indicated that the addition of nano-WO_3 to concrete

improved the mass attenuation coefficients by up to 8.7% and 8.0% compared to micro-particles for the photons with the energy of 142 and 662 keV [19]. The comparison of our findings with the aforementioned studies revealed that the highest mass attenuation of composites occurred in low-energy photons with the higher concentration of fillers and smaller particle sizes [23].

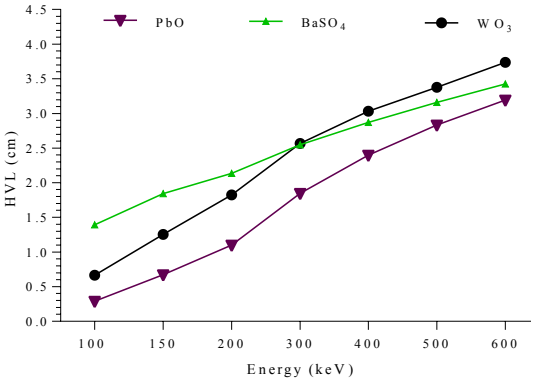

Fig 6. Comparison of HVL of Composites with PbO, $BaSO_4$, and WO_3 Nanoparticles at 40 wt% Concentration as Function of Photon Energy

Calculated MC half value layer of the studied nanocomposites

Fig 6 depicts the HVL of the samples with 40 wt% of filler concentration within the energy range of 100-600 keV. At a lower photon energy (100 keV), the HVLs were small and estimated at 0.29, 0.66, and 1.39 centimeters for the PbO, WO_3, and $BaSO_4$ composites, respectively. In addition, the HVL values increased at higher photon energies, and the HVL variation with the photon energy in these samples could be justified based on the dominance of various photon interaction processes in different energy regions as discussed above in the mass attenuation coefficients. Notably, lower HVL values were required for a better gamma-ray shielding material as it provided the higher probability of the photon interactions with the material. It was observed that the $BaSO_4$ composite had better shielding properties compared to the WO_3 and PbO composites at lower energies than 300 keV. Since the most effective shielding materials have lower HVL, the PbO 40wt% composite could be considered a proper candidate for photon attenuation purposes. The HVLs of 40 wt% PbO, $BaSO_4$, and WO_3 were estimated at 2.83, 3.16, and 3.37 centimeters for the γ-rays with the energy of 500 keV. In comparison with clinically used aprons, the narrow-beam HVLs of Pb aprons is 4.1 millimeters for photons with the energy of 511 keV [24]. Based on the shielding characteristics of the 40 wt% PbO composite, it could be selected as a proper alternative to conventional lead aprons.

Overall, our findings indicated that the developed metal matrix composite shields could be used for different applications in nuclear medicine departments in the form of apron shield (clothing) for the radiation protection of staff and patients, shielding material for the transfer of radioactive sources, and an isolation material in radioactive waste management facilities.

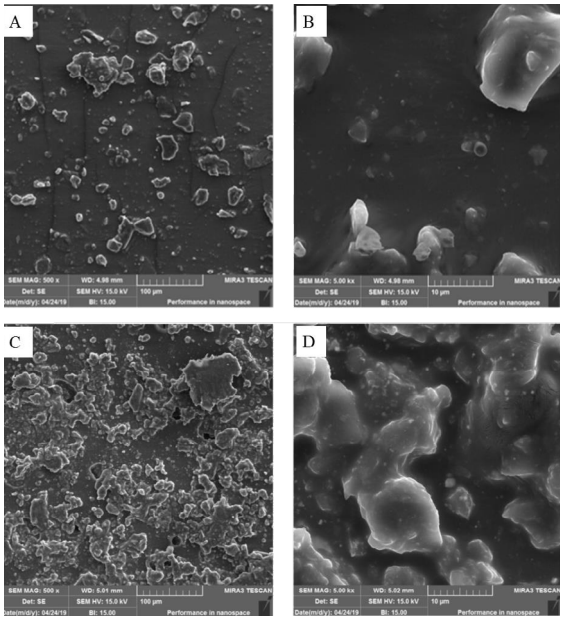

Fig 7. SEM Images of PbO and WO_3 Particles in Liquid Silicon Rubber Matrix; A and B) With Less Magnification and More Magnification of 10% PbO Composites, C and D) With Less Magnification and More Magnification of 10% WO_3 Composites

Material characterization

Fig 7 shows the SEM morphologies of the LSR of the composites containing the micro- and nano-PbO and WO_3 particles. The particle sizes of PbO and WO_3 varied from 50 to 200 nanometers. It is important for radiation protection materials to maintain proper dispersion and adhesion to prevent radiation from the shell interface and agglomerates that increase empty volumes. As is depicted in Fig 6, the PbO and WO_3 particles were properly dispersed inside the LSR matrix, and the particles were also homogeneous and bonded strongly in/with the LSR matrix.

In the current research, the EDS analysis was applied to measure the components of the

composite shields, and the spectra are shown in Fig 8.

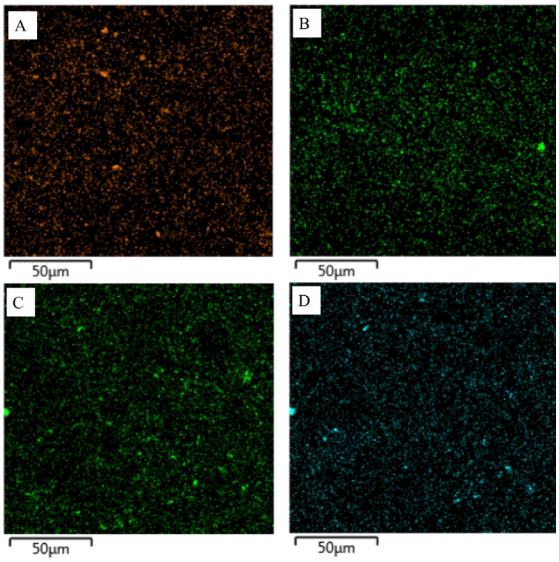

Fig 8. SEM-EDS Images of PbO and WO3 Particle Distribution in Liquid Silicon Rubber Matrix; A and B) 10% and 20% PbO Composites, C and D: 10% and 20% WO3 Composites

Through the spectra, the presence of PbO and WO_3 was observed in the composites. The EDS images of the PbO and WO_3 components in the composite shields at the ratios of 10% and 20% indicated their proper distribution in the LSR matrix.

DISCUSSION

Table 3 shows the results of the present study regarding the radiation protection properties of the composites with 10% and 20% concentrations of nano-PbO and nano-WO_3. Accordingly, the linear attenuation coefficient (μ) of the pure silicon rubber had the lowest value compared to the other samples.

As was expected, with the lower energy of the Am-241 photons (59.54 keV) in all the samples, the μ value was significantly higher compared to the Cs-137 photons (662 keV). This finding could be attributed to the dominance of the photoelectric effect at low energies where attenuation largely depends on the atomic number of the elements (~Z^3).

In contrast, at the higher energy of 662 keV, the Compton scattering effect was observed to be the most probable interaction between the photons and atoms, and the probability was based on the electron density of the materials. However, the composites with a low filler ratio (e.g., fabricated samples), the electron density had no significant changes.

Therefore, no significant changes were observed in the linear attenuation coefficients of the samples for the photons with the energy of 662 keV. Notably, the radiation protection properties of the composites increased at higher PbO and WO_3 concentrations.

Table 3. Radiation protection properties of the investigated samples determined by our experiments

MC	Experimental				
Mass Attenuation Coefficient (cm^2/g)	HVL (cm)	Mass Attenuation Coefficient (cm^2/g)	Linear Attenuation Coefficient (1/cm)	Radioactive Source	Samples
0.282	2.20	0.263	0.315	Am-241	100% Si rubber
0.128	5.13	0.113	0.135	Cs-137	
0.338	1.64	0.324	0.421	Am-241	10% WO_3
0.116	5.58	0.096	0.124	Cs-137	
0.396	1.30	0.373	0.533	Am-241	20% WO_3
0.109	5.33	0.091	0.130	Cs-137	
0.476	1.17	0.451	0.590	Am-241	10% PbO
0.115	5.21	0.102	0.133	Cs-137	
0.689	0.73	0.653	0.946	Am-241	20% PbO
0.111	4.74	0.101	0.146	Cs-137	

In addition, the PbO composites had higher linear attenuation coefficients compared to the WO_3 composite shields at the same energy and concentration. Table 3 shows the calculated MC results regarding the mass attenuation coefficients. Evidently, an average of 10% difference was observed between the MC and experimental results, which could be attributed to the non-homogeneity in the dispersion and particle size of the nanoparticles in the fabricated samples, while in the MC simulation, they were simulated completely homogenously with constant sizes.

The findings of the current research indicated the better radiation shielding of the NP-based composites, which could be attributed to the size effect. To clarify the effect, it could be stated that for the same mass ratio of the particles in the composites, the number of the NPs was 10^9 times higher than the micro-particles, and the NP multilayers were fixed together to block the radiation beams, which in turn led to the smaller voids between the NPs. In addition, the multiple scattering of the photons increased with the increased number of the particles, which made the pathway of the γ-ray photons longer, thereby leading to the higher photon absorption or decreased mean free path (MFP). The MFP denotes the average distance between two successive interactions of γ-rays. In the case of larger particles, the voids between the particles were larger, and less multiple scattering of γ-rays occurred due to the small number of the particles. In order to achieve the same shielding effect, more particles should be used to cover the interparticle spaces to increase scattering, which could cause the mass increase of the composite.

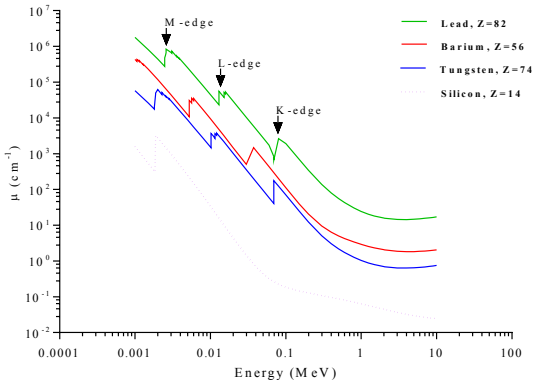

Fig 9. Linear Attenuation Coefficients of Used Elements in Energy Range of 1 keV-10 MeV Based on WinXCom Data

Fig 9 demonstrates the linear attenuation coefficient of Pb, Ba, W, and Si at various energies from 1 keV to 10 MeV using WinXCom. Basically, the photons were mainly absorbed by the photoelectric effect at lower energies, and the probability of the photoelectric effect partly depended on Z^3/E^3, where *Z* is the atomic number of the absorbing element, and *E* shows the photon energy [25]. Therefore, the photon attenuation ability of the studied composites prominently decreased with the photon energy due to the strong energy dependence of the photoelectric effect. Meanwhile, the increased photon energy resulted in the dominant effect of Compton scattering. As a result, the high-energy photons were generally attenuated by the materials through several rounds of Compton scattering, and the scattered photons with lower energy were eventually absorbed through the photoelectric effect.

As can be seen in Fig 9, the values decreased in the high-energy region, and 'sudden jumps' occurred at the energy of 100 keV. These 'sudden jumps' could be explained based on the absorption edges of the Pb, Ba, W, and Si elements. The incident photon energy corresponding to the absorption edges of the Pb element appeared at K (80.00 keV), L (15.90 keV), and M (13.00 keV), while the K-absorption edge of W, Ba, 80% W, and Si occurred at the energies of 69.5, 37.40, 69.50, and 1.870 keV. Furthermore, the increased photon energy from 0.1 to 0.8 MeV led to a significant decrease in the μ values as observed in the composite samples. This finding could be justified based on the dependence of the cross-section of the photoelectric process, which varied inversely with the photon energy as E^{-3} [26].

CONCLUSION

In the current research, the attenuation coefficients of silicon rubber-based composites containing 10%, 20%, and 40% of $BaSO_4$, WO_3, and PbO were calculated using the MCNP-X and WinXCom data. Moreover, the size effect of the $BaSO_4$, WO_3, and PbO particles on the shielding properties provided by nano-structured and micro-structured composites was investigated at the photon energies of 60, 80, 100, 150, 200, 300, 400, 500, and 600 keV. The PbO and WO_3 NPs were also synthesized rapidly and easily using a chemical method. Following that, LSR-based composites with 10% and 20% PbO and

WO_3 were manufactured using weighted shields. The mass attenuation coefficients of the PbO-LSR composites and WO_3-LSR composite shields were obtained by ^{137}Cs and ^{241}Am. According to the results, in the case of $BaSO_4$, WO_3 and PbO, the nano-sized particles had more significant attenuation properties compared to the micro-sized particles. Moreover, the composites doped with PbO significantly improved the shielding properties compared to $BaSO_4$ and WO_3 within the range of nuclear medicine energies. The comparison of the HVL results also indicated that the introduced composite shields with the higher ratio of the nano-particles could be used as an alternative to common lead shields.

ACKNOWLEDGMENTS

The authors would like to thank Medical Radiation Sciences Research Team, Tabriz University of Medical Sciences for support (Ethical Code: IR.TBZMED.REC.1396.1030).

REFERENCES

1. Ell PJ, Gambhir S. Nuclear medicine in clinical diagnosis and treatment. Churchill Livingstone. 2004.
2. Mettler A, Bhargavan M, Faulkner K, Gilley D, Gray J, Ibbott G, Lipoti J, Mahesh M, McCrohan JL, Stabin M. Radiologic and nuclear medicine studies in the United States and worldwide: frequency, radiation dose, and comparison with other radiation sources 1950–2007. Radiology. 2009; 253(2): 520-531.
3. Rangacharyulu C, Roh C. Isotopes for combined PET/SPECT imaging. J Radioanal Nucl Chem. 2015; 305(1): 87-92.
4. Madsen M, Anderson J, Halama J, Kleck J, Simpkin D, Votaw J, Wendt R, Williams L, Yester M. AAPM task group 108: PET and PET/CT shielding requirements. Med Phys. 2006; 33(1): 4-15.
5. Mattsson S. Introduction: The Importance of Radiation Protection in Nuclear Medicine. In: Radiation Protection in Nuclear Medicine. 2013; Springer: 1-3.
6. Huang B, Law M, Khong P. Whole-body PET/CT scanning: estimation of radiation dose and cancer risk. Radiology. 2009; 251(1): 166-174.
7. Ahasan M. Assessment of radiation dose in nuclear medicine hot lab. Inter J Radiat Res. 2004; 75-78.
8. Soylu H, Lambrecht F, Ersöz O. Gamma radiation shielding efficiency of a new lead-free composite material. J Radioanal Nucl Chem. 2015; 305(2): 529-534.
9. Mehnati P, Malekzadeh R, Sooteh MY, Refahi S. Assessment of the efficiency of new bismuth composite shields in radiation dose decline to breast during chest CT. Egypt J Radiol Nucl Med. 2018; 49(4): 1187-1189.
10. Mehnati P, Yousefi Sooteh M, Malekzadeh R, Divband B. Synthesis and characterization of nano Bi2O3 for radiology shield. Nanomed J. 2018; 5(4): 222-226.
11. Cataldo F, Prata M .New composites for neutron radiation shielding. J Radioanal Nucl Chem. 2019; 1-9.
12. Mehnati P, Malekzadeh R, Yousefi Sooteh M. New Bismuth composite shield for radiation protection of breast during coronary CT angiography. Iran J Radiol. 2019; 16(3).
13. Verdipoor K, Alemi A and Mesbahi A. Photon mass attenuation coefficients of a silicon resin loaded with WO3, PbO, and Bi2O3 Micro and Nano-particles for radiation shielding. Radiat Phys Chem. 2018; 147: 85-90.
14. Mehnati P, Sooteh MY, Malekzadeh R, Divband B, Refahi S. Breast conservation from radiation damage by using nano bismuth shields in chest CT scan. Crescent J Med Biol Sci. 2018; 6 (1): 46-50.
15. Mahmoud ME, El-Khatib AM, Badawi MS, Rashad AR, El-Sharkawy RM, Thabet A. Fabrication, characterization and gamma rays shielding properties of nano and micro lead oxide-dispersed-high density polyethylene composites. Radiat Phys Chem. 2018; 145: 160-173.
16. Mesbahi A, Alizadeh G, Seyed-Oskoee G, Azarpeyvand A. A new barite–colemanite concrete with lower neutron production in radiation therapy bunkers. Annal Nucl Energ. 2013; 51: 107-111.
17. Sayyed M, Issa SA, Tekin H, Saddeek Y. Comparative study of gamma-ray shielding and elastic properties of BaO–Bi2O3–B2O3 and ZnO–Bi2O3–B2O3 glass systems. Material Chem Phys. 2013; 217: 11-22.
18. Malekzadeh R, Mehnati P, Yousefi Sooteh M, Mesbahi A. Influence of size of nano and micro-particles and photon energy on mass attenuation coefficients of bismuth-silicon shields in diagnostic radiology. Radiol Phys Technol. 2019; 12(1): 6-25.
19. Mesbahi A, Ghiasi H. Shielding properties of the ordinary concrete loaded with micro-and nano-particles against neutron and gamma radiations. Appl Radiat Isot. 2018; 136: 27-31.
20. Berger M (2010) XCOM: photon cross sections database. http://www nist gov/pml/data/xcom/index.
21. Mehnati P, Malekzadeh R, Divband B, Yousefi Sooteh M. Assessment of the effect of nano-composite shield on radiation risk prevention to Breast during computed tomography. Iran J Radiol. 2020; 17(1).
22. Tekin H, Sayyed M, Issa S. Gamma radiation shielding properties of the hematite-serpentine concrete blended with WO3 and Bi2O3 micro and nano particles using MCNPX code. Radiat Phys Chem. 2018; 150: 95-100.
23. Mehnati P, Malekzadeh R and Sooteh MY. Use of bismuth shield for protection of superficial radiosensitive organs in patients undergoing computed tomography: a literature review and meta-analysis. Radiol Phys Technol. 2019; 12(1): 6-25.
24. Kim JY, Ahn S, Lee W. Shielding 140 keV gamma ray evaluation of dose by depth according to thickness of lead shield. J Radiol Sci Technol. 2018; 41(2): 129-134
25. Gaikwad D, Sayyed M, Obaid SS, Issa SA, Pawar P. Gamma ray shielding properties of TeO2-ZnF2-As2O3-Sm2O3 glasses. J Alloy Compoun. 2018; 765: 451-458
26. Mesbahi A. A review on gold nanoparticles radiosensitization effect in radiation therapy of cancer. Rep Pract Oncol Radiother. 2013; 15(6): 176-180.